

Gennaro Barbato, Giuseppe Pezzella & Antonio Viviani

Università della Campania "Luigi Vanvitelli", Dipartimento d'Ingegneria. Via Roma 29, I-81031 Aversa (CE), Italy.

#### **Abstract**

This paper deals with the conceptual design of an unmanned aerial vehicle, suitable for Mars surface exploration activities. A propeller-driven configuration, powered by solar panels and batteries, and equipped with a fixed-wing is investigated. Specifically, a multidisciplinary design tool for the preliminary sizing of a Martian rectangular wing is proposed. After establishing the mission requirements and selecting the technological parameters, the research objective is to analyze how the optimum wing design point, in terms of wingspan and aspect ratio, varies as aerodynamic coefficients and payload mass change. The optimal sizing is chosen based on UAV gross mass and range. The proposed design procedure relies on the power and mass balances that occur during level flight. The design tool enables the determination of design requirements in terms of Reynolds and Mach numbers at cruising flight conditions. The in-house developed tool and its design results are detailed discussed in the paper.

Keywords: Mars exploration aircraft, Preliminary design, Design Requirements, Design Constraints.

## 1. Introduction

The concept of designing a drone capable to fly in the Martian atmosphere was first proposed in 1977, when Chirivella, from JPL (NASA), was tasked with developing a drone for the Earth upper atmosphere [1]. Upon realizing the similarities between the aerodynamic conditions of the Earth stratosphere and the Martian atmosphere, it became evident that a fixed-wing drone could be utilized also to explore Mars. The first drone to satisfy the Martian flight requirements was the Mini-Sniffer [2, 3]. A second Unmanned Aerial Vehicle (UAV) prototype was born in 1978, when Clarke et al. [2] proposed the Astroplane. From 1980 to 2005, in addition to NASA, various universities and industries became involved in similar research activities. Among the most notable configurations proposed, there were the AME prototype of 1996, developed by the AMES Research Center of NASA [4], the CanyonFlyer designed by Smith [5], and the MarsFlyer of Aurora Flight Sciences (1999) [6], the ARES-2 proposed by Guynn (NASA) [7] in 2003, and the Sky-Sailor of the Autonomous Systems Lab of European Space Agency (ESA) in 2004 [8]. The advent of new technologies, including propulsion systems, composite materials, energy storage and production systems, has enabled the introduction of innovative configurations, such as inflatable wing, flapping-wing, and rotary-wing drones, as well as aerostatic drones and solar-powered drones with foldable wings. To date, only the NASA Ingenuity drone has successfully completed an atmospheric flight in the Martian environment. The primary challenge of Martian flight is producing enough lift to support an aircraft with a substantial scientific payload. Currently, drones are a popular choice for exploring Mars due to their higher spatial resolution compared to orbiters and greater range than rovers. Fixed-wing configurations are very attractive for their high range and ability to carry a larger scientific payload [1]. Therefore, the next objective in Martian exploration activities is to propose a fixed-wing configuration capable of flying for a longer duration [9] [10] [11].

The ultimate goal is to lay the groundwork for a possible future human mission to Mars. The present research work is framed within this context.

# 2. Martian Atmospheric Environment

The Martian atmosphere presents a challenging aerodynamic environment, with Reynolds number of the order of 10<sup>4</sup> and sound speed close to 240 m/s at 1 km altitude. The low values of the Reynolds number are mainly caused by an average density that reaches 0.015 kg/m<sup>3</sup> on the Martian surface, which is roughly two orders of magnitude lower than that on Earth. The typical cruising conditions on Mars are like that of the Earth upper stratosphere, at about 30 km altitude (i.e., the stratospheric layer) [12]. The low Reynolds numbers result in decreased aerodynamic efficiency, which negatively impacts on aircraft performance. This leads to a non-linear behavior of aircraft lift coefficient, even at low attitude conditions, due to the laminar flow separation. The most challenging fluid dynamics phenomenon is the well-known Laminar Separation Bubble (LSB) [13]. Additionally, the low sound speed value causes compressibility effects to occur even at very low cruising speeds. On the red planet, solar radiation represents the sole available source of power. It diminishes in proportion to the square of the heliocentric distance. In Astronomical Units (Aus), Mars is situated on average at a distance of 1.52 AU from the Sun. Consequently, solar radiation is less prevalent than on Earth. The Martian environment also features atmospheric winds. The wind speeds increase during the dust storm season in the autumn and winter months. The force of the Martian winds is an order of magnitude smaller than on Earth due to the lower atmospheric density. The so-called "Dust devils" on Mars have been observed to reach heights of several kilometers and rotate at speeds exceeding 30 m/s, with transverse speeds of over 15 m/s [14]. Such high-velocity wind formations would be problematic for the UAV if it were to be caught in one. The only positive feature of this challenging environment is the magnitude of the gravitational field. The total mass of Mars is less than that of the Earth, resulting in a gravitational acceleration of 3.72 m/s<sup>2</sup> on the Martian surface, which is approximately 39% of the terrestrial gravitational acceleration.

# 3. Conceptual Design Methodology

The primary objective of this research effort is to develop a multidisciplinary design tool for the preliminary sizing of UAV lifting surfaces. This work is framed within the conceptual design of a propeller-driven configuration, powered by solar panels and batteries, proposed for a long-range exploration activity of the Martian surface. The conceptual design procedure employed follows the Noth methodology, which was proposed for the design of the Sky-Sailor [15]. The aim of the research is to rework Noth's design procedure in order to determine the design requirements in terms of Reynolds and Mach numbers at cruising flight conditions and to evaluate the effect of wing size on drone endurance. The wing design parameters taken into account are aspect ratio (AR) and wingspan (b).

The design methodology is based on the power and mass balances that occur during level flight, as shown in the non-exhaustive flowchart in Figure 1. The surface imaging activities can be modelled as a fixed altitude cruise, during which the scientific payload requires a power supply. Therefore, the design starting point is represented by straight level flight conditions. The design tool has to satisfy two constraints:

- 1. Weight balance: the wing must produce enough lift to sustain the UAV configuration
- 2. **Power balance**: the power available must be equal or higher than electrical power needed by all the drone system (e.g., propeller, avionics and scientific payload)

The Noth methodology, as described in [15], was initially proposed for a solar powered drone designed to perform a powered continuous flight (from day to night and *vice versa*). To date, this ambitious goal remains unachievable with the current technological level, as Noth observed in his work [15]. The mentioned methodology implemented an integral constraint, that deals with the drone powered issue in term of energy balance (as opposed to power balance, as is proposed here). In the Noth methodology, the energy collected during all daylight hours must be equal to the electrical energy needed during the day, in addition to the energy required to charge the battery system. The batteries are responsible for supplying the energy required during the Martian night. In this research work, instead, a punctual constraint is implemented. The drone endurance is calculated as an output parameter, which depends on the configuration layout through level flight power.

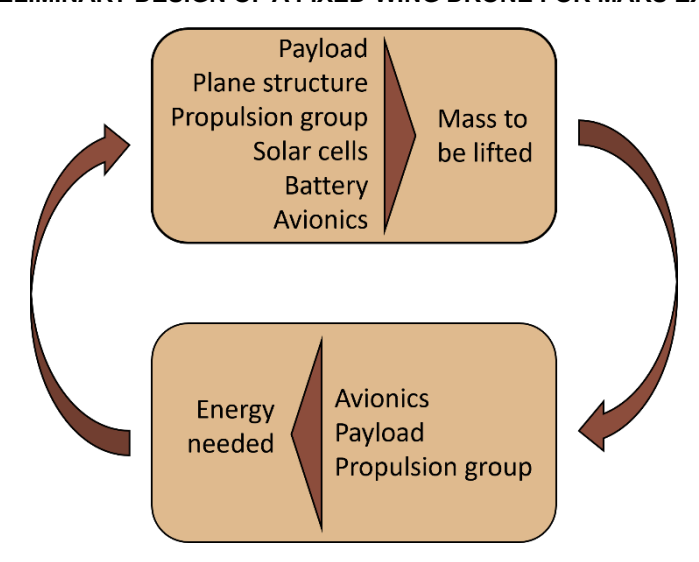


Figure 1: Design Methodology Flowchart

The high-level design capability of the tool must be framed within a conceptual design. The objective was to develop a useful tool to guide the selection of the wing design point and to provide the cruise conditions for the aerodynamic optimization of airfoil shape [10] [11] [10]. The tool has been developed in the MATLAB programming language and is structured in a way that allows for the straightforward incorporation of additional modules. An in-house aerodynamic module is currently under investigation.

# 3.1 UAV mass prediction

The total mass of the drone is calculated by summing the masses of its components, including payload and avionics, airframe, batteries, solar panels, and propulsion group.

$$m_{tot} = m_{af} + m_{sc} + m_{bat} + m_{prop} + m_{av} + m_{pld}$$
 (1)

The payload mass is assumed based on mission requirements. An example of imaging system is proposed by Collins et al. [14]. In order to perform surface exploration activities, a substantial scientific payload could be formed by two wide-angle cameras (downward and forward facing) and four narrowangle cameras (all downward facing). This system has a mass of approximately 1.3 kg. The sensitivity analysis presented herein considers a payload mass range consistent with the aforementioned value. The design tool implements both the payload and avionics mass as input parameters.

$$m_{pld} + m_{av} = const (2)$$

A realistic value for the UAV avionics mass is proposed by Collins [14] and Bertani [16]. A system comprising servos, a flight control board, sensors, wiring and a controller could have a mass of approximately 0.50 kg. In addition, the communications system must be considered, which could be represented by a low-gain antenna and UHF transceiver. Collins [14] propose a mass of 1.00 kg for this type of Martian drone subsystem.

The mass of the drone airframe is certainly the most challenging part to model and predict. Noth [15] proposed a new empirical model:

$$m_{af} = k_{af} b^{x_1} A R^{x_2} \tag{3}$$

The model was derived from a database containing 415 samples of sailplanes. In order to ensure that only the sailplanes with the best construction quality are considered, the fitting law is evaluated on the basis of only 19 samples (representing the top 5% of the entire database). The model coefficients were calculated using a least square fitting method. The values obtained are reported below.  $k_{af} = \frac{0.44}{9.81} \ kg/m^3 \qquad x_1 = 3.10 \qquad x_2 = -0.25$ 

$$k_{af} = \frac{0.44}{9.81} \, kg/m^3$$
  $x_1 = 3.10$   $x_2 = -0.25$ 

The propulsion group is composed of four subparts (i.e., control electronics, motor, gearbox, and propeller). A prevailing trend in the design of solar-powered aircraft is to assume a propulsion group mass that scales linearly with shaft power output. In consideration of all four subparts, Noth in [15] proposed a mass-to-power ratio for the entire propulsion group, namely:

$$m_{prop} = k_{prop} P_{lev} k_{prop} = 0.008 \ kg/W (4)$$

The mass of the solar panel is calculated using the following equation, where  $k_{sc}$  and  $k_{enc}$  represent the surface density of the solar cells and the encapsulation, respectively. In order to design a UAV capable of continuous flight, Noth in [15] considers the exact percentage of the wing required to balance the electrical energy consumed with the total electrical energy obtained from the sun. This approach is not so appropriate for the design of a Martian UAV, since a 24-hour continuous flight is not yet feasible. Instead, in this work it is assumed that the covered wing area  $S_{sc}$  is equal to 90% of the wing area  $S_{cc}$ :

$$m_{sc} = S_{sc} (k_{sc} + k_{enc})$$
  $S_{sc} = 0.90 S$  (5)

The performance of the solar panels is evaluated by reference to the CTJ30 model, as proposed by Bertani [16]. The CTJ30 is a triple-junction solar cell for space applications developed by CESI. It is composed of multiple layers made of indium-gallium-phosphorus (In-GaP), gallium arsenide (GaAs), and germanium (Ge). This type of flexible solar cell can be mounted on the upper surface of a cambered wing and is characterized by a very low areal density of approximately 500 g/m².

In the design loop, the battery mass is introduced as an input parameter. The mass of the battery is proportional to the stored energy, and thus linked to the drone endurance. A larger battery can store more energy, but this results in an increase in the configuration gross mass. In order to sustain a heavier configuration, it is necessary to fly faster, which in turn increases the dynamic pressure and drag force. To perform a non-accelerated cruise condition with a larger asymptotic speed, the propeller requires more power, which has a negative effect on the drone's endurance. Therefore, increasing the battery mass is not always a beneficial strategy. In the present work, a sensitivity analysis was conducted to identify the optimal battery size for each layout. The correlation between stored energy and battery mass can be expressed as follows:

$$m_{bat} = \frac{1}{k_{bat}} E_{storage} \tag{6}$$

in which  $k_{bat}$  is the battery energy density. The proposed configuration is developed to perform a single long-range mission. Thus, the current version of the tool provides a primary battery. The specific energy is evaluated by reference to the Li-SOCl<sub>2</sub> system (400 Wh/kg) [17].

## 3.2 Required electrical power

The energy required to power the drone is calculated by adding the power needed for horizontal flight (minus the efficiency of the electric thruster components), the power needed to operate the onboard avionics, the scientific payload, and the communications system. As suggested by Noth in [15], if the voltage of these elements must be reduced, the efficiency of the step-down  $\eta_{bec}$  has to be considered. This gives the following total electrical power consumption:

$$P_{tot} = \frac{1}{\eta_{prop}} P_{lev} + \frac{1}{\eta_{bec}} \left( P_{av} + P_{com} + P_{pld} \right) \tag{7}$$

The power consumption of the avionics  $P_{av}$ , the payload instruments  $P_{pld}$  and the communications system  $P_{com}$  is computed as an input parameter. The sources of electrical energy are the solar cells and the batteries. The power produced by the solar cells is estimated by multiplying the incident solar radiation with the area of the solar cells, their conversion efficiency  $\eta_{sc}$  and the efficiency  $\eta_{mppt}$  of the MPPT. In addition, we have to take into account the fact that the cells are not installed on a horizontal surface but follow the cambered airfoil. To take this effect into account, Noth proposed a new efficiency  $\eta_{cbr}$ . The electrical power produced by the solar cells is thus estimated as follows:

$$P_{sc} = I S_{sc} \eta_{sc} \eta_{cbr} \eta_{mppt}$$
 (8)

The CTJ30 solar cell has a declared efficiency of 29.5% at 1367 W/m² and 25°C. In order to account for the low temperature on Mars, the cell efficiency is assumed to be equal to 20%, as proposed by Bertani [16]. Solar radiation depends on many variables such as geographic location, time, plane orientation, weather conditions and albedo. In the presented tool, the available solar radiation is estimated by using the values suggested by the Mars Climate Database [18]. The orientation of the solar cell array is modelled as a stationary horizontal surface on the Martian soil. The research deals with the conceptual design of a subsonic UAV configuration, so the wing surface of the drone can be assimilated to a stationary surface. The electrical energy extracted from the battery is lower than that is stored, because the discharge efficiency must be taken into account. This leads to the following relation:

$$E_{bat} = \eta_{dchrq} E_{storage} \tag{9}$$

The UAV endurance is calculated as the mission time during which the total required power is less than or equal to the available electrical power. The available power is based on the solar cells and battery contribute. Introducing a solar radiation profile, the drone endurance is calculated by adding the rate supplied by the battery to the endurance guaranteed by the solar panels.

## 3.3 Aerodynamic performance estimation

The assessment of wing aerodynamic performance represents a challenging task. In the Martian atmosphere, the UAV must perform a level flight in low Reynolds conditions. The aerodynamic performance is dominated by the viscosity effects due to laminar separation, with pressure drag representing the predominant contribution within the drag computation. Hence, the proposed aerodynamic coefficients must take into account the viscosity effect. The examined tool aims to evaluate a preliminary wing sizing and its optimal cruise conditions; thus, a preliminary estimation of the wing performance is derived empirically from that of the equipped airfoil. Specifically, a low-fidelity drag breakdown method is proposed. As suggested by Spedding in [19], at low Reynolds numbers, the appropriate expression for a wing drag coefficient estimation would be of the form:

$$C_D = C_d + \frac{C_L^2}{\pi \ AR \ e_i}$$
  $C_d = C_d(C_l)$  (10)

in which  $e_i$  is only the correction for nonelliptic loading, and  $\mathcal{C}_d$  is the two-dimensional airfoil drag. An initial value of  $\mathcal{C}_d$  is computed for the appropriate angle of attack from 2D drag polars. With the proposed approach, the viscous airfoil drag, and the inviscid induced drag are kept separate. In order to account for the parasitic drag resulting from non-lifting parts, such as the fuselage or the tail, the total drag coefficient is calculated as the sum of three contributions:

$$C_{Dtot} = C_{Dpar} + C_D = C_{Dpar} + C_d + \frac{C_L^2}{\pi AR e_i}$$
 (11)

where the parasitic drag coefficient  $C_{Dpar}$  is considered as a constant input parameter. The value suggested by Noth [15] of 65 counts is computed.

The integration of an airfoil into a finite-size wing inevitably results in a deterioration in its aerodynamic performance. Regarding the lift curve, the finite aspect ratio results in a reduction in the airfoil's capacity to generate lift. A preliminary value, to be proposed as input to the design procedure, is calculated from the two-dimensional lift coefficient. A first attempt can be expressed through empirical reduction as follows:

$$C_L = 0.90 \cdot C_l \tag{12}$$

where  $C_L$  represents the lift coefficient of the finite wing and  $C_l$  that of its equipped airfoil.

## 3.4 Design problem modelling

In this framework, the design problem is solved using a third-degree equation in the variable  $z=m^{1/2}$ :

$$\alpha(AR, b)z^3 - z^2 + \beta(AR, b) = 0$$
 with  $z = m^{1/2}$  (13)

The coefficients of the third-degree equation depend firstly on the two design parameters (as well as other fixed parameters, see below): aspect ratio, *AR*, and wingspan, *b*.

The code solves an equation like the one shown, and it reports all feasible combinations (AR, b) that result in a positive real root. It should be noted that the design model equation depends on more than 25 parameters, which can be divided into three different classes:

- a) Technology parameters, linked to the technological level of each drone component;
- b) Mission parameters linked to the mission requirements and the atmospheric conditions on Mars (i.e., the geographical location and the time of the solar year);
- c) Design parameters, which are the optimization objectives related to the aerodynamic layout of the rectangular wing area.

After establishing the mission requirements and selecting the technological parameters, various wing layouts can be tested by adjusting the design parameters to determine the optimal configuration that

satisfies the power and mass balance previously mentioned. The employed approach is an analytical and continuous approach, which consists in establishing all the relations between the components with analytical equations. This method directly provides a unique and optimized design, but it does require accurate mathematical models [15]. The developed tool is able to evaluate and collect the feasible wing layout. Subsequently, a Pareto front is generated from the collected solution set. The target features are gross mass and range. For illustrative purposes, an example is presented in Figure 2.

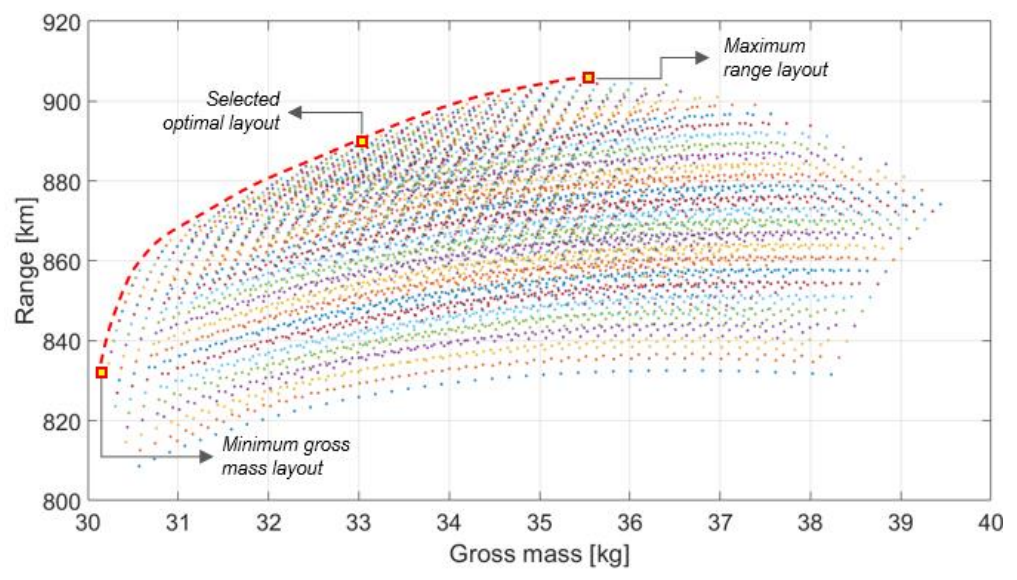


Figure 2: Design candidates on Pareto front.

The Pareto front is constituted by different sets of curves, each of which is calculated with a distinct battery mass (points marked in the same color represent wing layouts with same aspect ratio). In order to select the optimal layout, an objective function is defined as follows:

$$f(AR,b) = a_1 \cdot Gross \, Mass + a_2 \cdot \frac{1}{Range} \tag{14}$$

The optimal layout is evaluated by calculating the minimum of the objective function.

## 4. Design Methodology Application

In this section is proposed an exploratory analysis in order to evaluate the optimal wing size for a long-range mission in the Martian atmosphere at rather low altitude (i.e., 1 km). In particular, the inhouse developed design tool has been used to identify the flight conditions in terms of Reynolds and Mach number, and to obtain an initial estimation of UAV mission capabilities (e.g., gross mass, range, endurance, and power needed). The proposed results also aim to evaluate the effects of the aerodynamics coefficient on the wing design. The subsequent section elucidates the rationale behind the mission site selection and delineates the parameters used to determine the appropriate time of year. This is followed by a brief aerodynamic characterization of the E387 airfoil that has been preliminary selected for the proposed exploratory analysis.

## 4.1 Mission Location and year period

The Martian plain *Isidis Planitia* has been selected as exploration region for the UAV example mission, as proposed by Collins [14]. The *Isidis Planitia* region is an ideal operating environment for the UAV, offering a multitude of advantages from both a scientific and engineering point of view. The plain is large and fairly circular with a low latitude and low elevation. Due to its proximity to the Martian equator, the solar radiation will hit on the drone's solar cells at a higher angle, generating more power than at higher latitudes. The lower elevation will aid the UAV while flying due to the higher atmospheric density. Furthermore, the inner portions of the plain are relatively flat, which is beneficial for the UAV's planned flight path. *Isidis Planitia* is also an excellent candidate to carry out new science missions on Mars. It is the third largest impact crater on Mars, and it is thought to have

contained water at one time. The reference coordinates used are 13.56°N 88.22°E. A Mars topographic map is reported in Figure 3 [16].

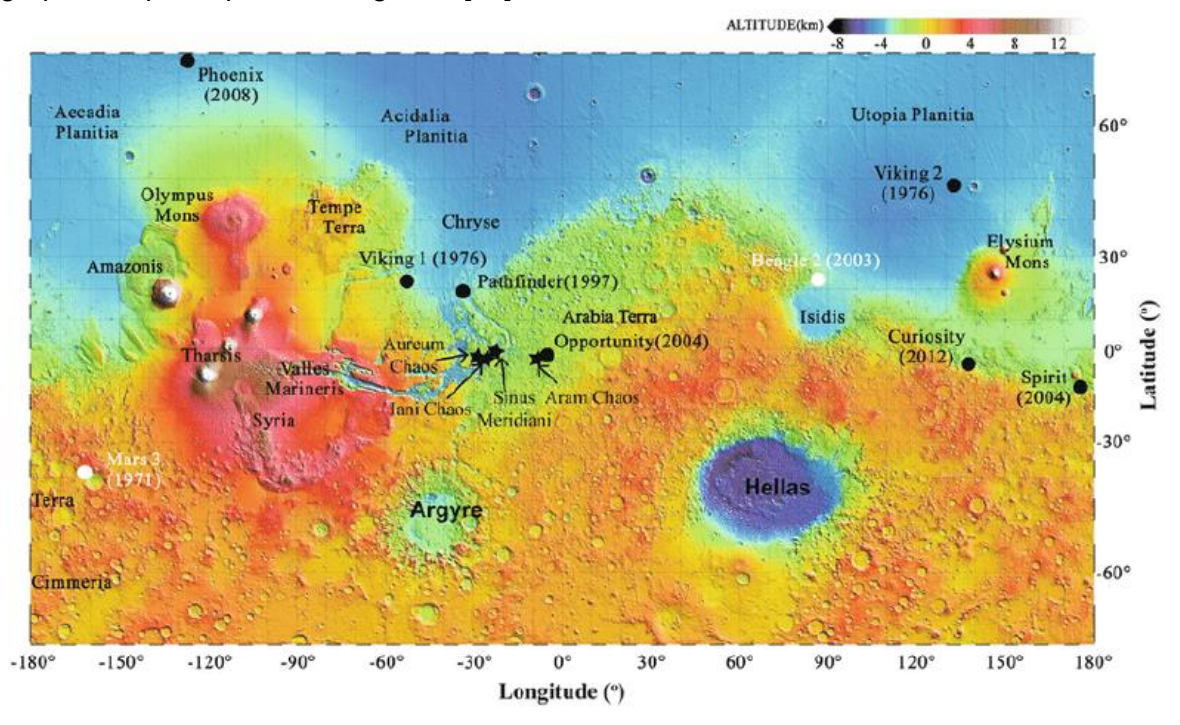


Figure 3: Mars topographic map [16].

Based on the calculated predictions from the Mars Climate Database [18], the UAV should operate during the late spring or early summertime period and conduct mission close to local noon on *Isidis Planitia*. Operating outside of the dust storm season (fall and winter, from 180 to 360 degrees of aerocentric longitude) will minimize the probability of a dust storm occurring. Flying at local noon will ensure that the UAV is exposed to the maximum solar insolation during flight. The maximum incident solar flux at the top of the atmosphere and on the horizontal surface varies throughout the Martian year, as illustrated in Figure 4

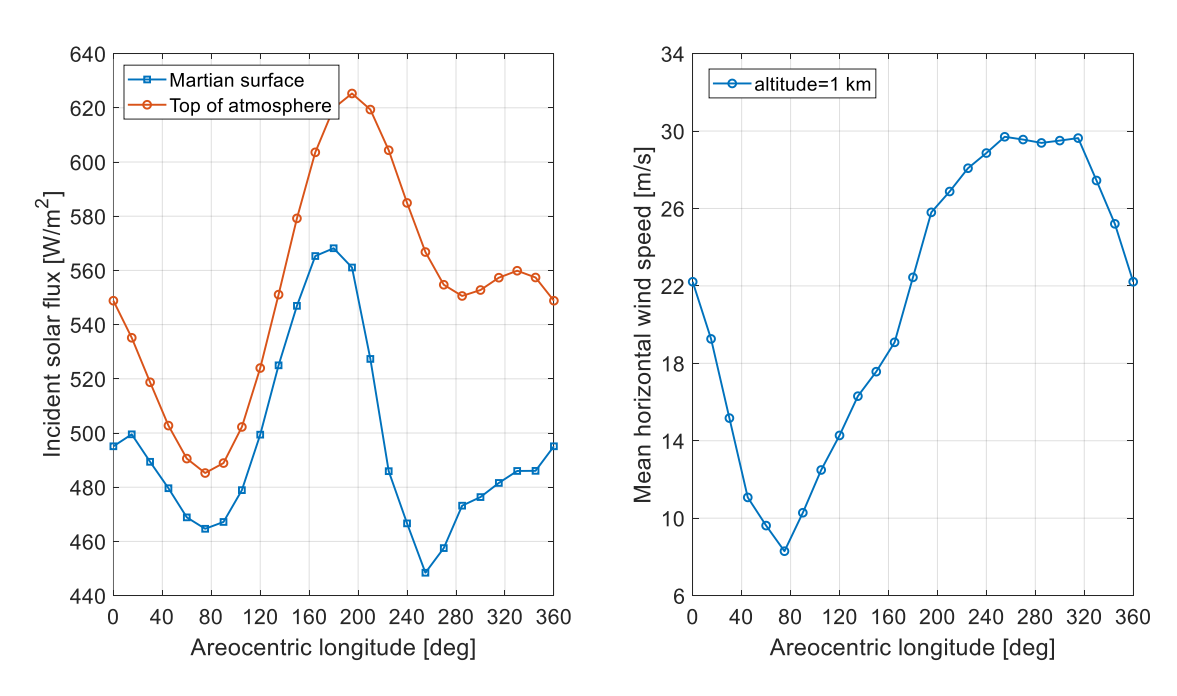


Figure 4: Solar insolation and mean wind speeds for Isidis Planitia during Martian year.

Due to the highly eccentric orbit of Mars and to the different average climate conditions, the maximum solar flux variation is approximately 21%. The intensity of solar radiation reaching the surface is significantly reduced during dust storms, resulting in a substantial reduction in drone solar-energy generation capability. Within the aerocentric longitude range from 0 to 180 degrees, the maximum solar flux on horizontal surface is reached during the Northern Hemisphere Autumn Equinox (Ls=180°). In Figure 4, the mean horizontal wind speed recommends conducting flight missions in close to the Northern Hemisphere Summer Solstice (Ls = 90°). In this paper, an exploration mission in the *Isidis Planitia* at Ls=150° is proposed as a trade-off choice. Average daily wind speeds and solar insolation during local time (Martian hour) are illustrated in Figure 5.

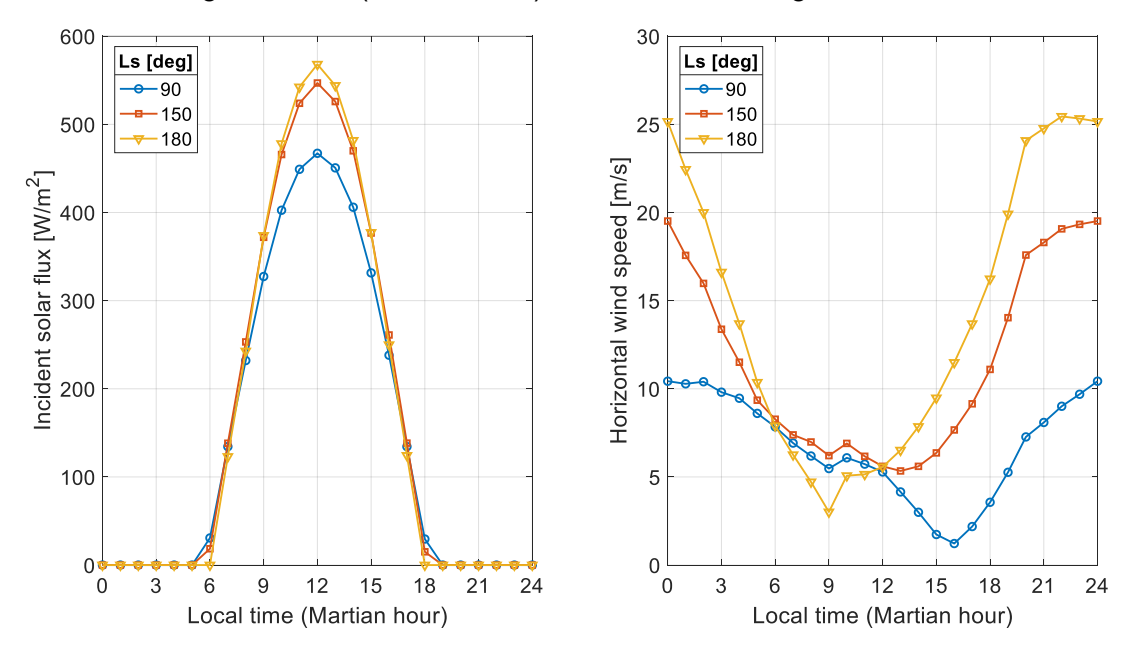


Figure 5: Daily solar insolation and wind speeds for *Isidis Planitia*.

## 4.2 Two-dimensional wing section

For the purposes of this design methodology application, the selected airfoil is the Eppler-387. It is a well-known laminar profile, designed for incompressible flight conditions at low Reynolds regime. The profile exhibits a thickness distribution with a maximum value of 9.1% at 31.1% of the chord. The maximum curvature is 3.2% and is situated at 44.8% of the chord. Anyway, further design assessments involving in-house developed optimized airfoil are under investigation and results provided in future work [10] [11].

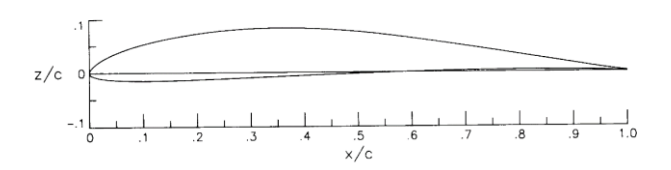


Figure 6: Eppler-387 airfoil [20].

## 4.2.1 Low Reynolds aerodynamic performance

In order to examine the tool design capabilities, the Wind Tunnel (WT) data in [20] were selected as a reference point for the assessment of airfoil aerodynamic performance. The tests were conducted at a Reynolds number of  $60x10^3$  in the Langley Low-Turbulence Pressure Tunnel (Virginia, USA), the Model Wind Tunnel in Stuttgart (Germany) and the Low-Turbulence Tunnel in Delft (Netherlands). The Figure 7 presents a comparison between the aforementioned WT data and the numerical results obtained with Xfoil.

The proposed WT results show a marked difference in profile aerodynamic performance. This result is not surprising, given that these are fluid-dynamic phenomena closely related to the behavior of the

laminar boundary layer. The sensitivity of the laminar boundary layer to free-stream disturbances, tunnel conditions and model surface roughness is considerable [20].

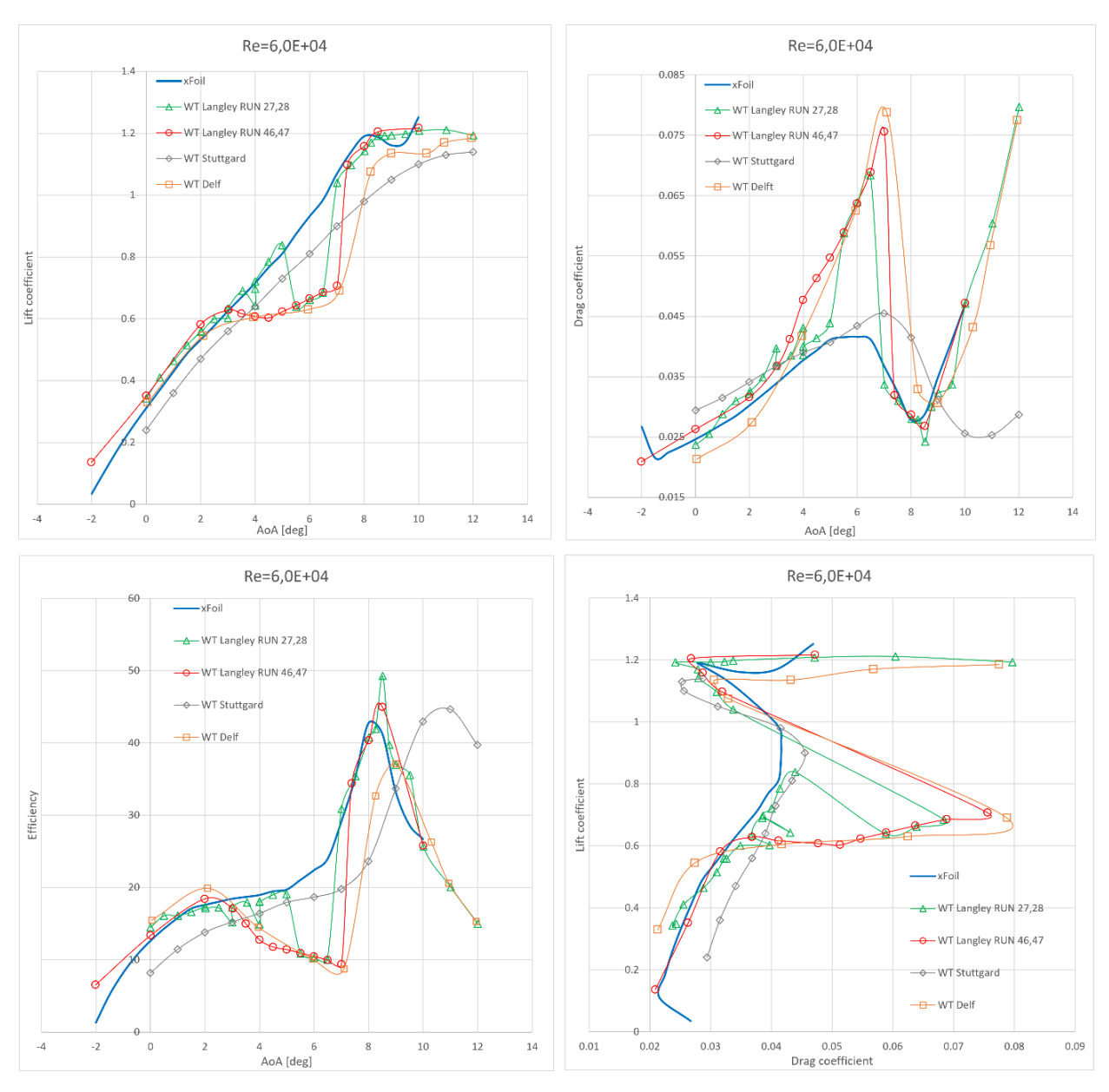


Figure 7: E387 aerodynamic coefficients (Re=60x10<sup>3</sup>) [20].

The LTPT RUNs 27 and 28 (M=0.16 and turbulence level of 0.16%) indicate a strong non-stationary flow condition, which occurs at AoA between 3 and 7 degrees. In particular, two distinct scenarios are observed: laminar flow separation with and without turbulent reattachment. Instead, a stable flow field in RUNs 46 and 47 is produced. These are tunnel simulations performed with a higher turbulence level (approximately 0.20%) and a slightly higher incompressible Mach number (M=0.09). In these conditions, a laminar separation is observed within the 3-7° range. At larger angles of attack (after 7.5°), a consistent flow reattachment is observed for both tunnel conditions (RUN 27,28 and RUN 46,47). Figure 7 provides a further comparison with the results from the Stuttgart and Delft tunnels, where the free-stream turbulence level is 0.08% and 0.03%, respectively. The LTPT and Delft data demonstrate a laminar stall with  $C_1 \approx 0.6$  and a reattachment occurring near  $C_1 = 1.05$ . Conversely, the Stuttgart WT measurements do not exhibit any phenomena related to LSB failed reattachment. The numerical results demonstrate a satisfactory agreement with the LTPT data outside the laminar stall region. In fact, it is evident that the Xfoil analysis is unable to capture the failure of boundary layer reattachment. A more detailed comparison is proposed with the pressure coefficient distributions shown in Figure 8.

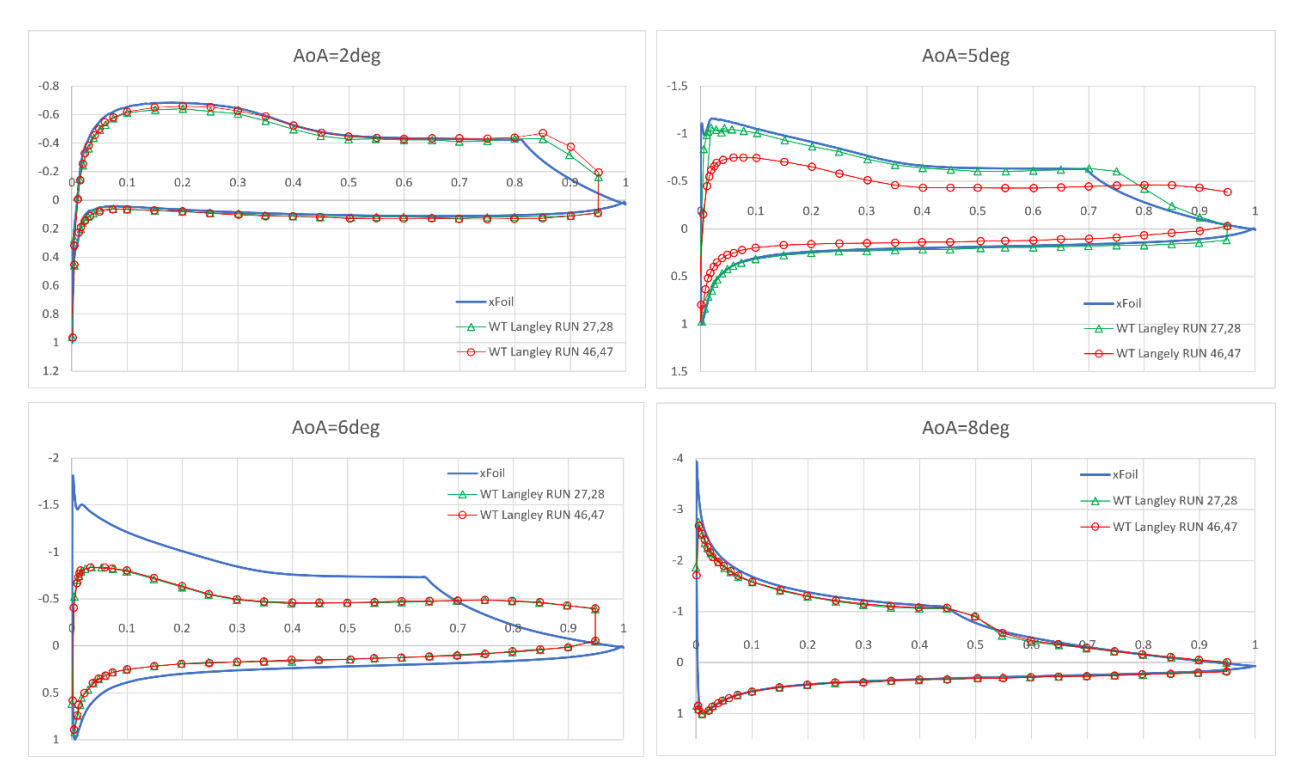


Figure 8: Pressure coefficient distributions ( $\alpha$ =2,5,6,8 deg Re=60x10<sup>3</sup>) [20].

As one can see, Xfoil is able to successfully describe the presence of a laminar bubble, and its extension variation as the angle of attack,  $\alpha$ , increases. At  $\alpha$ =2° and  $\alpha$ =8°, the  $c_p$  distribution calculated by Xfoil is consistent with the LTPT experimental evidence (RUN 27,28 and RUN 46,47). At  $\alpha$ =5°, there is a satisfactory reproduction of RUN 27,28 and a markedly disparate trend from that of RUN 46,47 (where turbulent reattachment does not occur). At  $\alpha$ =6°, the distribution reconstructed by Xfoil differs from both tunnel curves. In order to identify realistic aerodynamic coefficients for input to the design procedure, the focus is on the maximum aerodynamic efficiency point, where the prediction of Xfoil and LTPT are in agreement. Therefore, aware of the Xfoil prediction limits, an exploratory analysis about the maximum aerodynamic efficiency around Re=60x10³ is carried out. Figure 9 provides a summary of the results obtained. The numerical results indicate a comparable trend to that previously discussed up to a Reynolds number of approximately 50x10³. As the Reynolds number decreases, the reliability of numerical predictions becomes increasingly questionable. Traub and Coffman [21] have observed that at Re=40x10³, Xfoil predictions are not reliable. The maximum efficiency trend in Figure 9 has been completed with WT data presented in [22].

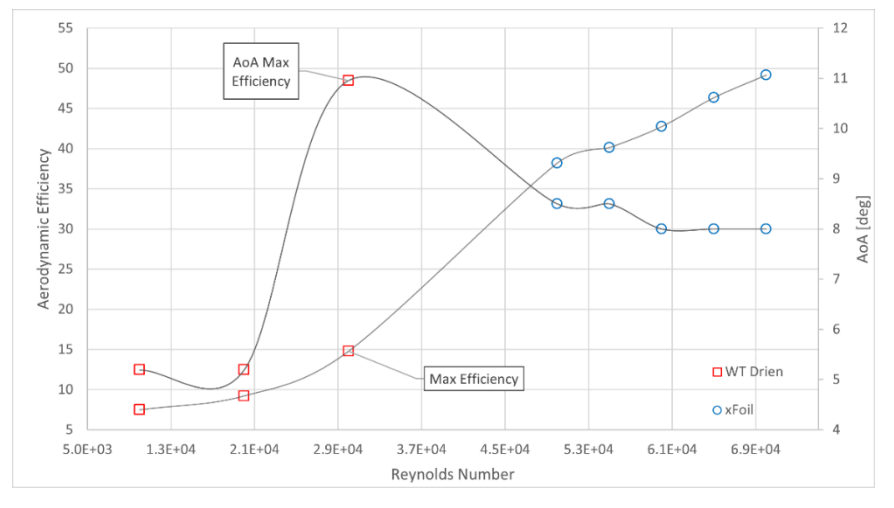


Figure 9: E387 aerodynamic efficiency [22].

Within a narrow range of Re=60x10³, the selected reference values (see Figure 8) are expected to provide an accurate order of magnitude for 2D aerodynamic performance. The tool's design capabilities were tested by taking the performance at Re=60x10³ as a reference. Consequently, the validity range of the tool results is constrained by the aerodynamic coefficients variability. The proposed objective is to demonstrate the high-level design capabilities of the tool. A plug-in aerodynamic module is still under investigation; its discussion and implementation are deferred to future work.

#### 4.2.2 Critical Mach Number

The critical lower Mach number represents the threshold value at which the effects of compressibility become significant, and a sonic velocity point emerges in the flow field. To obtain an initial estimate of this threshold value, it is possible to refer to the minimum pressure coefficient point that is realised around the airfoil in incompressible condition. Subsequently, the critical lower Mach is estimated by calculating the asymptotic Mach at which the minimum  $c_p$ , corrected for the effect of compressibility, reaches the sonic value. In order to calculate the effects of compressibility on  $c_p$ , the Laitone correction was used [23]:

$$c_{p}\big|_{M_{\infty}} = \frac{c_{p}\big|_{M_{\infty}=0}}{\sqrt{1 - M_{\infty}^{2}} + \frac{c_{p}\big|_{M_{\infty}=0}}{2} \frac{M_{\infty}^{2} \left(1 + \frac{\gamma - 1}{2} M_{\infty}^{2}\right)}{\sqrt{1 - M_{\infty}^{2}} + 1}$$
(15)

In order to calculate the sonic value of the pressure coefficient, Anderson [23] proposes the following isentropic relation:

$$c_{p \ crit} = \frac{2}{\gamma M_{\infty}^2} \left( \left( \frac{2 + (\gamma - 1)M_{\infty}^2}{\gamma + 1} \right)^{\frac{\gamma}{\gamma - 1}} - 1 \right)$$
 (16)

Consequently, the incompressible flowfield around the E387 profile was evaluated using Xfoil, resulting in the outcomes depicted in Figure 10.

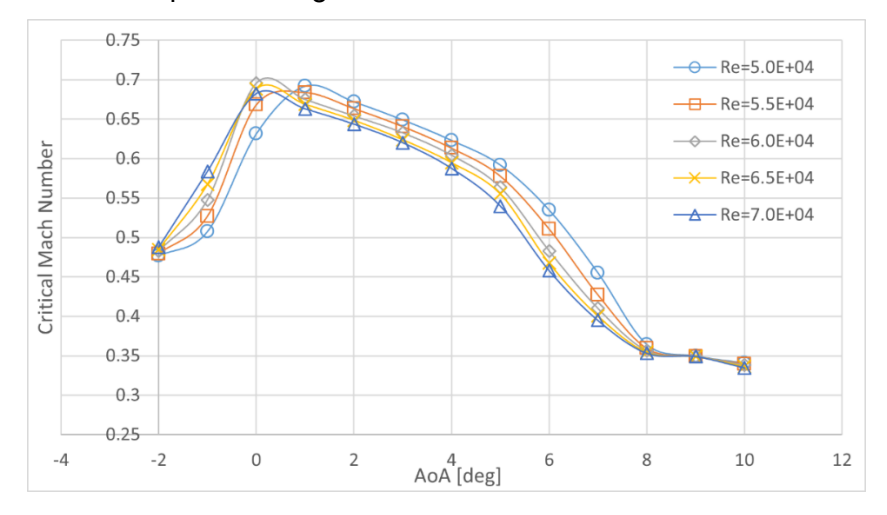


Figure 10: E387 critical Mach number

#### 4.3 Numerical Results

Once the technological parameters have been set and the mission and design parameters chosen, it was possible to collect the tool output data and analyse the proposed trends. In order to evaluate the lifting capability of a fixed rectangular wing, the value proposed by Eq. (12) was taken as a reference, exploring a range of lift coefficient around the latter. Figure 11, Figure 12 and Figure 13 show the results thus obtained. Recall that in these figures, the blue curve refers to  $C_L$ =0.9, the red one to  $C_L$ =1.0, and that yellow to  $C_L$ =1.1.

A brief commentary on the trends proposed by the tool will now be presented.

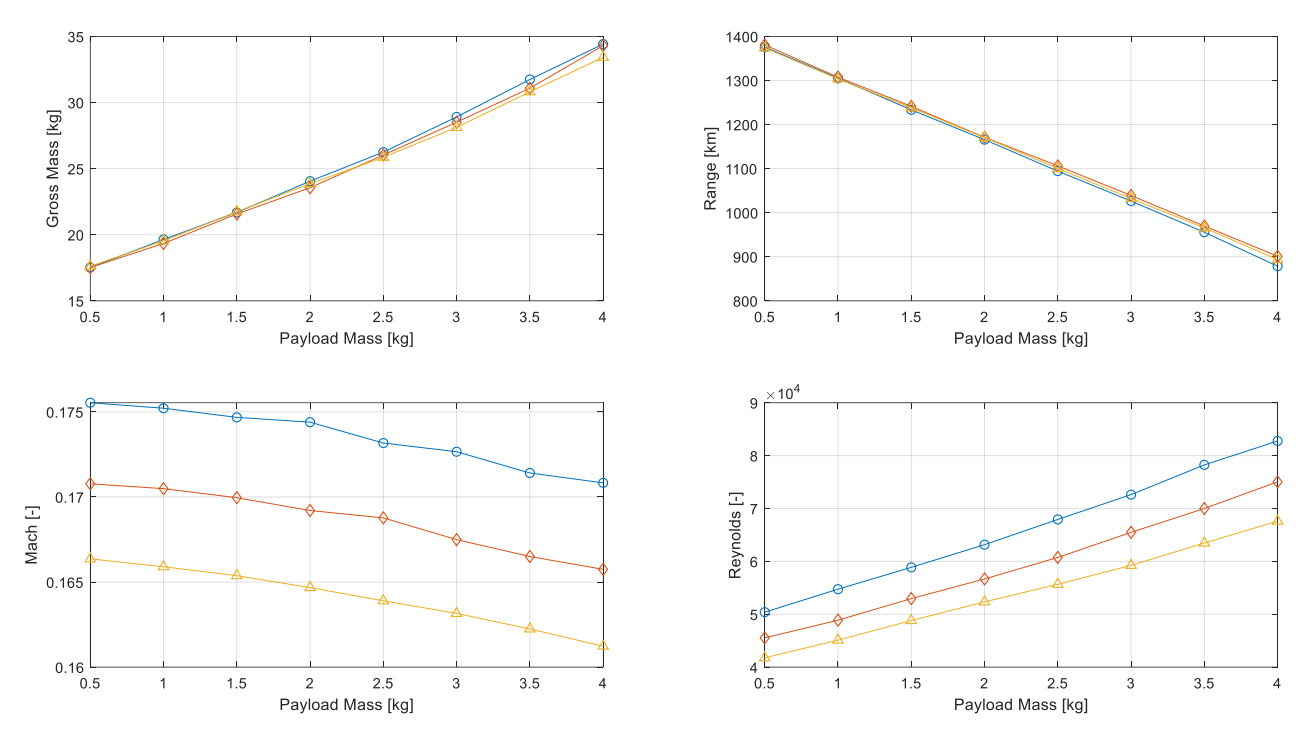


Figure 11: Drone and level flight characteristics depending on payload mass and lift coefficient. The blue curve refers to  $C_L$ =0.9, the red one to  $C_L$ =1.0, and that yellow to  $C_L$ =1.1.

It can be reasonably assumed that the lift capacities are sufficient to sustain a UAV configuration equipped with a scientific payload of 0.5 to 4kg. As might be expected, the mass of the configuration increases with the payload. A gross mass range of approximately 17 to 35kg is expected. For a payload of 2kg, the estimated mass is perfectly in line with the Halcyon and Hyperion configurations [14]. This estimate is promising because, assuming the weight of the communications system (1kg) is added to the scientific payload (2kg), the predicted configuration will carry a fixed mass of 3kg, as planned for Halcyon and Hyperion. The trends in Figure 11 indicate that the gross mass is not affected by the lift coefficient. This result can be justified by observing that as the lift coefficient decreases, the necessary wing area increases but the optimal aspect ratio decreases (wing planforms with low aspect ratio are lighter) and the optimal battery system equipped is lighter (see Figure 12 and Figure 13).

The cruising Mach trend in Figure 11 indicates optimal speeds that respect the compressibility constraint (see Figure 10). The reported cruising speeds are minimally affected by the payload carried, exhibiting a maximum variation of 2.3 m/s due to lift coefficient. It is evident that the lift force increase required due to an increase in payload (and/or a decrease in lift coefficient) is mainly compensated for by an increase in wing area.

The predicted cruising conditions for the various layouts are expected to have a Reynolds number of  $10^4$  order of magnitude. Once the flight altitude has been established (1 km), Reynolds number changes should be correlated with variations in speed and, in particular, the increase in the wing chord (see Figure 13). The reference aerodynamic performance is that of the E387 airfoil, which refers to a Reynolds number of  $60x10^3$ . The trends in Figure 11 indicate that an E387-like airfoil could be used for a long-range mission with a 2kg payload, drawing on an optimum cruise Reynolds of approximately  $60x10^3$ .

The reduction in the estimated UAV range as the payload increases is a consequence of endurance reduction. The diagram in Figure 12 indicates a low sensitivity to the lift coefficient.

A wing configuration that equips an E387-like airfoil, carries a 2kg payload and operates at 60x10<sup>3</sup> cruise Reynolds number would be able to perform an imaging exploration activity and cover up to 1160km. This is an optimistic estimate, because it does not take into account the effect of atmospheric winds.

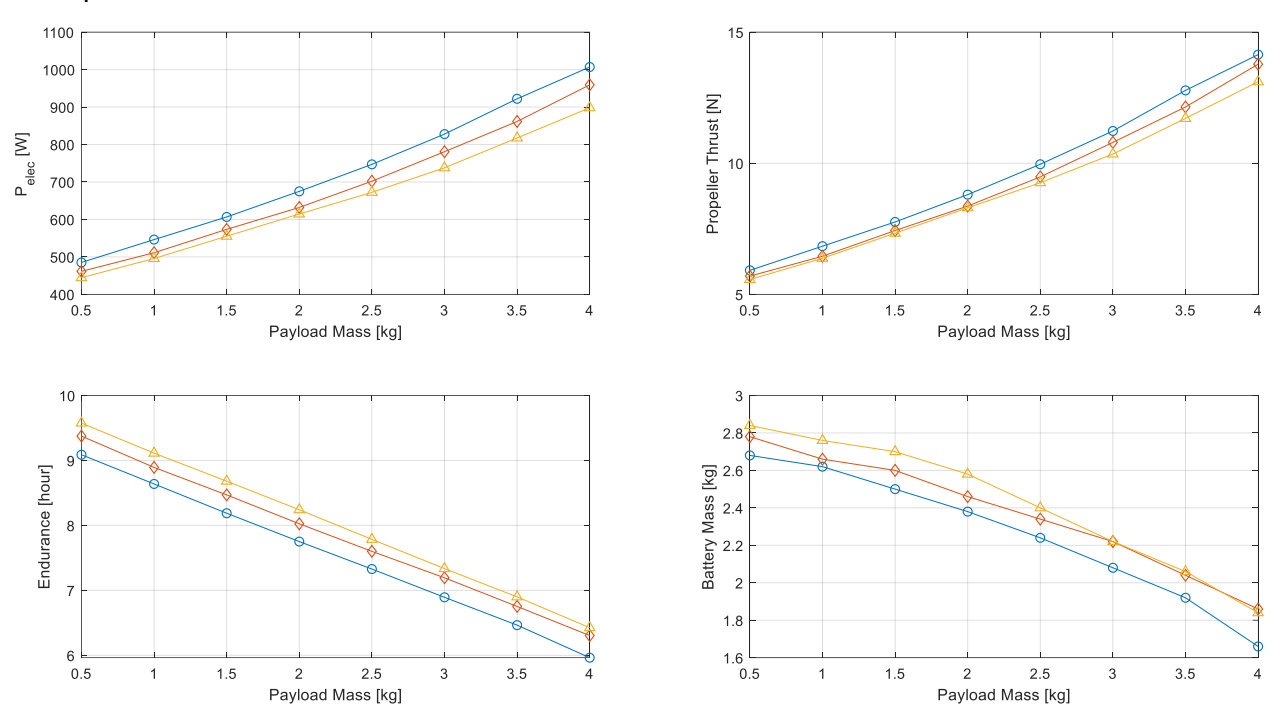


Figure 12: Power supply parameters depending on payload mass and lift coefficient. The blue curve refers to  $C_L=0.9$ , the red one to  $C_L=1.0$ , and that yellow to  $C_L=1.1$ .

Figure 12 illustrates a trend of increasing required electrical power due to payload increases. This is to be expected, given that as the UAV gross mass increases, the wing area becomes larger and the optimal aspect ratio decreases (see Figure 13).

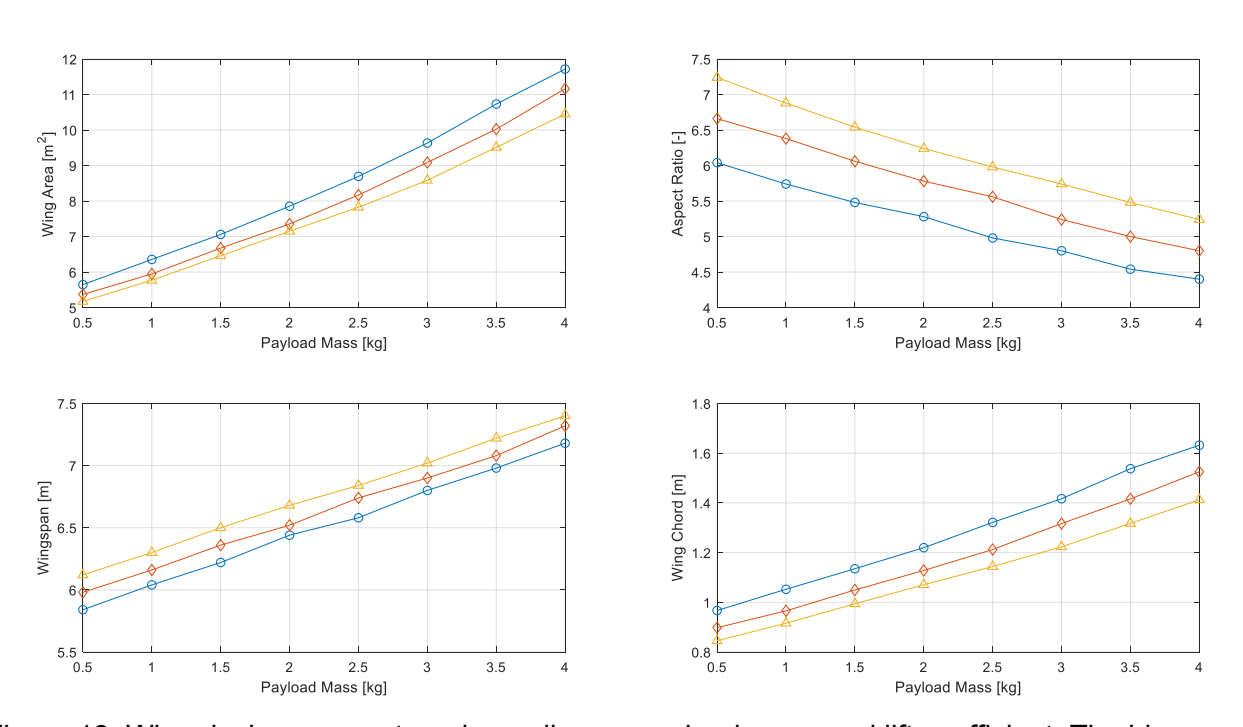


Figure 13: Wing design parameters depending on payload mass and lift coefficient. The blue curve refers to  $C_L$ =0.9, the red one to  $C_L$ =1.0, and that yellow to  $C_L$ =1.1.

This results in an increase in drag force, which in turn increases propeller thrust. Conversely, an increase in the lift coefficient results in a significant reduction in required power. Preliminary estimates indicate that the power required to perform a long-range exploration mission with a payload of 2kg is approximately 635÷680W.

This range is close to Collins' power estimate of 710W for the cruise operations [14].

The drone's endurance is closely related to the electrical power consumption, so it decreases as the payload increases. The rate of decrease in endurance is less than that in electrical power. This is because as the wing area increases, the area covered by the solar panels also increases, resulting in an increase in the produced electrical energy.

The proposed results show that the optimal battery mass is between 1.65kg and 2.85kg. In order to limit the increase of the gross mass, as the payload carried increases, it is advisable to equip the UAV with a lighter battery (conversely as the lift factor rises).

Given that the optimal cruising speed varies slightly, the wing surface area has to change in order to ensure sufficient lift force for sustenance.

The aspect ratio is highly sensitive to the lift coefficient. As the lift coefficient increases, the optimal aspect ratio shifts towards higher values in order to limit the induced drag. Conversely, as the carried scientific payload increases, the optimal aspect ratio decreases because the optimum design point shifts towards lighter wing planforms.

For a long-range exploration activity with a payload of 2kg, the optimal planform has an aspect ratio between 5.3 and 6.3. The results indicate a low sensitivity of wingspan to the lift coefficient. Given a payload of 2kg, an optimal wingspan range is 6.45 to 6.68m.

## 4.3.1 Martian fixed-wing UAV comparison

Tennekes [24] demonstrated, in his renowned Great Flight Diagram, that flying bodies on Earth exhibited a fundamental scaling law based on their velocity, wing loading, and mass, as illustrated in Figure 14. Nevertheless, Noth's investigation of sailplanes revealed that not all manmade aircraft adhere to this simple scaling law.

Light, high aspect ratio aircraft deviate from Tennekes' model and exhibit a shift to the left of the trend line. A limited number of proposed fixed-wing Martian UAVs are overlayed onto the Great Flight Diagram by Collins, which demonstrates that all of the Martian drones are shifted to the left of Tennekes' model.

Furthermore, Collins observed that the high-speed designs are more consistent with Noth's model than the low-speed proposal [14].

The proposed configuration for a 2kg payload mission can be overlayed onto the Great Flight Diagram in Figure 14 adapted from Collins [14].

This allows an insight to be gained into the specific design region identified by the tool. The proposed layout has a gross mass of 23.86kg, which is slightly lower than that of the Halcyon & Hyperion (25kg), while the wing loading (12.07N/m²) is intermediate between that of the Halcyon & Hyperion (11.27N/m²) and the Mars Solar Aircraft (12.65N/m²).

One of the main steps in the design process of space drones is the wing sizing, which effects the aeroshell packaging, the gross mass, the aerodynamic and exploration performance. In the proposed tool, the analysis is carried out considering the gross mass and the exploration capability. The layout effects on the aerodynamic performance are evaluated through a low-fidelity approach. The plug-in aerodynamic module under investigation aims to improve this tool limitation.

In any case, a comparison with other fixed-wing Martian UAVs could provide some preliminary information, as reported in Figure 15.

As one can see, present design results are perfectly in trend with those available in literature, thus highlighting the reliability of the multidisciplinary design tool.

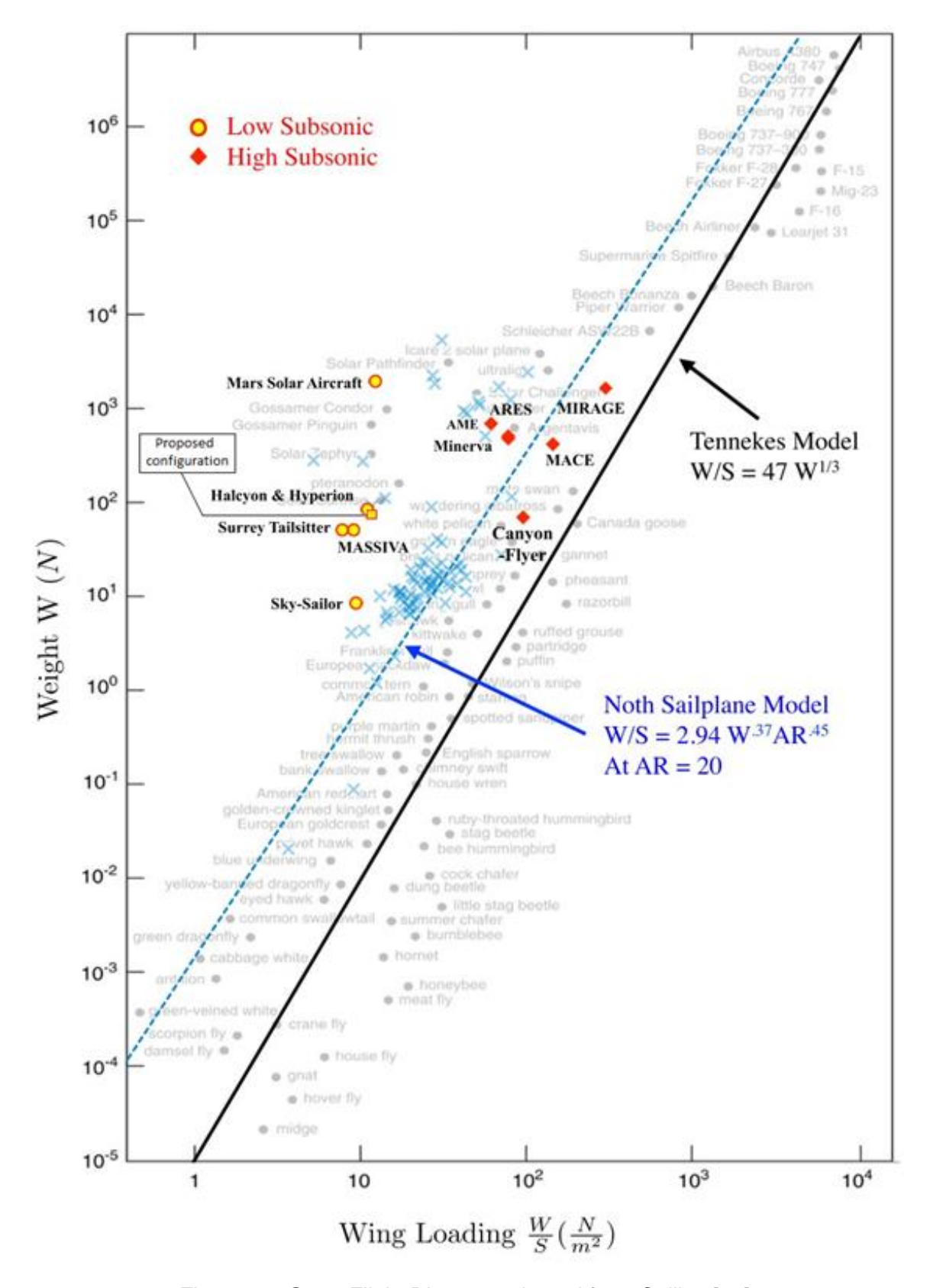


Figure 14: Great Flight Diagram adapted from Collins [14].

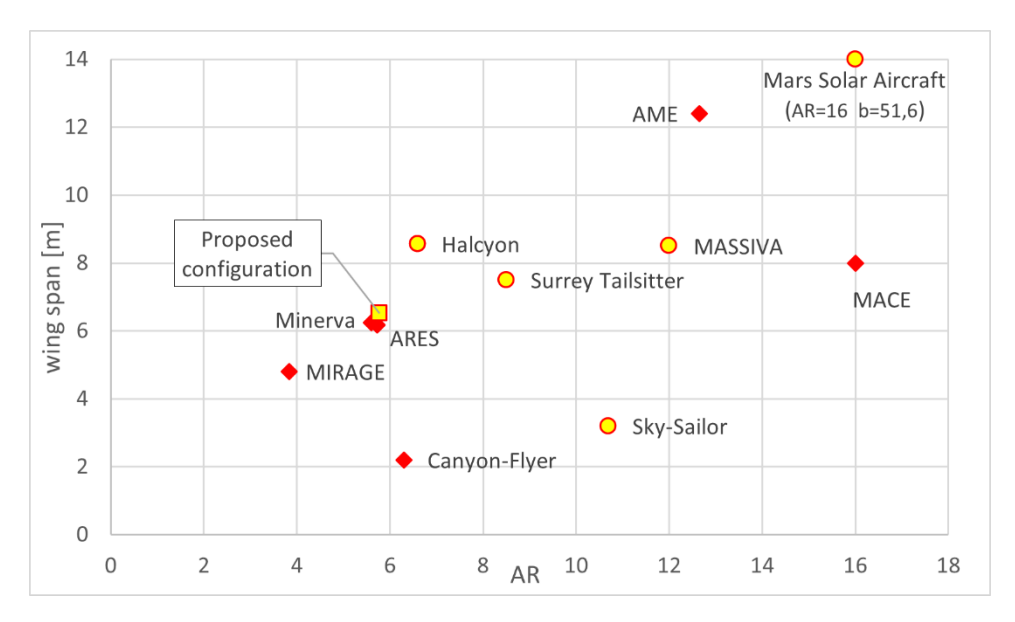


Figure 15: wingspan and aspect ratio of the Martian configuration (database Collins [14]).

#### 5. Conclusions

This paper dealt with the conceptual design of a unmanned aerial vehicle, suitable for Mars surface exploration activities. A propeller-driven configuration, powered by solar panels and batteries, and equipped with a fixed-wing was investigated. Specifically, a multidisciplinary design tool for the preliminary sizing of a Martian rectangular wing was presented. After establishing the mission requirements and selecting the technological parameters, the research objective analyzed how the optimum wing design point, in terms of wingspan and aspect ratio, varies as aerodynamic coefficients and payload mass change. The optimal sizing was chosen based on UAV gross mass and range. The proposed design procedure was linked to the power and mass balances that occur during level flight. Finally, the discussed design tool enabled the determination of design requirements in terms of Reynolds and Mach numbers at cruising flight conditions. The in-house developed tool and its design results are detailed discussed in the paper.

#### 6. Contact Author Email Address

E-mail address: antonio.viviani@unicampania.it

## 7. Copyright Statement

The authors confirm that they, and/or their company or organization, hold copyright on all of the original material included in this paper. The authors also confirm that they have obtained permission, from the copyright holder of any third party material included in this paper, to publish it as part of their paper. The authors confirm that they give permission, or have obtained permission from the copyright holder of this paper, for the publication and distribution of this paper as part of the ICAS proceedings or as individual off-prints from the proceedings.

#### References

- [1] M. Hassanalian, D. Rice e A. Abdelkefi, «Evolution of space drones for planetary exploration: A review,» *Progress in Aerospace Sciences*, vol. 97, pp. 61-105, 2018.
- [2] V. J. Clarke, A. Karem e R. Lewis, «A Mars Airplane... Oh really?,» American Institute of Aeronautics and Astronautics, New Orleans, 1979.
- [3] R. D. Reed, «High-flying Mini-Sniffer RPV Mars bound,» *Astronautics and Aeronautics*, vol. 16, 1978.
- [4] A. A. Gonzales, C. J. Corpus, D. W. Hall e R. W. Parks, «Developement of a useful Mars airplane exploration concept at NASA/Ames Research Center,» in *6th Mars Society Conference*, 2003.
- [5] S. Smith, A. Hahn, W. Johnson, D. Kinney, J. Pollitt e J. Reuther, «The design of the Canyon Flyer, an airplane for Mars exploration,» in *38th Aerospace Sciences Meeting and Exhibit*, Reno NV, 2000.
- [6] D. D. Walker, «Preliminary Design, Flight Simulation, and Task Evaluation of a Mars Airplane,» 2008.
- [7] M. Guynn, M. Croom, S. Smith, R. Parks e P. Gelhausen, «Evolution of a Mars Airplane Concept for the ARES Mars Scout Mission,» in *2nd AIAA "Unmanned Unlimited" Conf. And Workshop & Exhibit*, 2003.
- [8] A. Noth, S. Bouabdallah, S. Michaud, R. Siegwart e W. Engel, «SKY-SAILOR Design of an autonomous solar powered martian airplane,» in *Proc. 8th ESA Workshop Advanced Space Technologies Robotics Automation (ASTRA 2004)*, Noordwijk, Netherlands, 2004.
- [9] A. Viviani, A. Aprovitola, L. Iuspa and G. Pezzella, "Optimization Procedure for a Wing of a Mars Exploration Drone," in *34th Congress of the International Council of the Aeronautical Sciences*, Florence, Italy., 2024.
- [10] A. Aprovitola, L. Iuspa, G. Pezzella e A. Viviani, «Aerodynamic optimization of airfoils shape for atmospheric flight on Mars planet,» *Acta Astronautica*, vol. 212, pp. 580-594, 2023.
- [11] A. Aprovitola, L. Iuspa, G. Pezzella and A. Viviani, "Flows past airfoils for the low-Reynolds number conditions of flying in Martian atmosphere," *Acta Astronautica,* vol. 221, p. 94–107, 2024.
- [12] A. J. Colozza, «Preliminary design of a long-endurance Mars aircraft,» in *26th Joint Propulsion Conference*, Orlando, FL, 1990.
- [13] J. Winslow, H. Otsuka, B. Govindarajan e I. Chopra, «Basic Understanding of Airfoil Characteristics at Low Reynolds Numbers (10^4-10^5),» *Journal of Aircraft*, vol. 55, n. 3, 2018.
- [14] N. S. Collins, «System Design and Nonlinear State-Dependent Riccati Equation Control of Autonomous Y-4 Tilt-Rotor Aerobot for Martian Exploration,» Guildford, 2016.
- [15] A. Noth, R. Siegwart, P. Corke, A. Borschberg and C. Nicollier, "Design of Solar Powered Airplanes for Continuous Flight," ETH Zurich, 2008.

- [16] M. Bertani e A. Guardone, «Preliminary design of a fixed-wing VTOL UAV for Martian flight,» 2023.
- [17] A. D. Pathak, S. Saha, V. K. Bharti, M. M. Gaikwad e C. S. Sharma, «A review on battery technology for space application,» *Journal of Energy Storage*, n. 61, 2023.
- [18] E. Millour, F. Forget, A. Spiga, M. Vals, V. Zakharov, L. Montabone, F. Lefèvre, F. Montmessin, J.-Y. Chaufray, M. A. Lopez-Valverde, F. Gonzalez-Galindo, S. R. Lewis, P. L. Read, M.-C. Desjean e F. Cipriani, «The Mars Climate Database (version 6.1),» Scientific Workshop: "From Mars Express to ExoMars", 27-28 Febbraio 2018. [Online]. Available: https://www-mars.lmd.jussieu.fr/mcd\_python/. [Consultato il giorno 26 11 2023].
- [19] G. R. Spedding e J. McArthur, «Span Efficiencies of Wings at Low Reynolds Numbers,» *Journal of Aircraft*, vol. 47, n. 1, 2010.
- [20] R. J. McGhee, B. S. Walker e B. F. Millard, «Experimental Results for the Eppler 387 Airfoil at Low Reynolds Numbers in the Langley Low-Turbulence Pressure Tunnel,» Langley Research Center, Hampton, 1988.
- [21] L. W. Traub e E. Cooper, «Experimental Investigation of Pressure Measurement and Airfoil Characteristics at Low Reynolds Numbers,» *Journal of Aircraft*, vol. 45, n. 4, 2008.
- [22] J. McArthur, «Aerodynamics of wing at low Reynolds Numbers,» University of Southern California, 2007.
- [23] J. Anderson, Fundamentals of Aerodynamics, New York: McGraw-Hill, 2017.
- [24] H. Tennekes, The Simple Science of Flight, London: Massachusetts Institute of Technology, 2009.